~~A-175~~
176

TANTALUM MICROSTRUCTURES FOR HIGH-STRAIN-RATE DEFORMATION: SHOCK LOADING, SHAPED CHARGES, AND EXPLOSIVELY FORMED PENETRATORS

L. E. Murr, S. Pappu, C. Kennedy, C-S. Niou, and M. A. Meyers*

Department of Metallurgical and Materials Engineering,
The University of Texas at El Paso, El Paso, TX 79968 and
*Department of Applied Mechanics and Engineering Sciences,
University of California, San Diego, La Jolla, CA 92093

Abstract

Deformation twins coincident with {112} planes have been observed by TEM to be generally profuse in annealed, tantalum plate with equiaxed grains roughly 45 μm in diameter subjected to a plane shock wave having a peak pressure of 45 GPa. Correspondingly, no deformation twin evidence was observed in either tantalum residual shaped charge microstructures (recovered jet fragments or slugs) or recovered EFP's, utilizing similar liner materials (annealed, equiaxed tantalum with grain sizes ranging from about 40 to 70 μm). Recovered shaped charge jet particles exhibited cross-section microstructures characterized primarily by very small grains and characteristic softening, indicative of dynamic recrystallization. There were often several concentric zones of varying, small grain size. Recovered shaped charge slugs exhibited a dynamically recrystallized central core region which evolved somewhat systematically into dynamically recovered microstructures consisting of elongated dislocation cells and becoming larger, more equiaxed cells; with decreasing angles of misorientation toward the slug perimeter. Recovered EFP microstructures exhibited mixtures of evolutionary dislocation and dislocation cell structures, including elongated, dynamic recovery cells with only very few indications of dynamic recrystallization in specific, corresponding, high-strain regions.

Introduction

Recently, tantalum, tungsten, and tantalum-tungsten alloys (up to about 10 wt percent W) have found applications in a variety of penetrating weapons and related ballistic devices primarily as a consequence of their high densities which promote more efficient armor penetration, which is related to $\sqrt{\rho_p/\rho_t}$; where ρ_p and ρ_t are the penetrator and target densities, respectively. In the more popular penetrator concepts such as shaped charges and explosively formed penetrators (EFP's), a dense metal liner, such as Ta, in conical and related, simple geometries, is initially subjected to a strong explosively-generated shock wave which then dynamically drives the subsequent penetrator development. In the shape-forming and self-forging processes which characterize these devices, metallurgical issues, especially the initial liner microstructures and their evolutionary development appear to play an important role in the stability of the device and the efficiency of the process up to cessation of penetration. It has already been demonstrated that liner microstructure issues, including grain size, stored energy of fabrication (prior deformation), and texture, can have significant effects on both shaped charge and EFP development and performance (1-6).

In this paper, we present a brief summary of some of the prominent microstructures and micro-structural variations observed in initial tantalum liners, a shock loaded liner material, recovered shaped-charge components (jet fragments and slugs), and EFP slugs.

Experimental Details

We examined a number of Ta liner discs, forged plates, and liner cones having equiaxed grain structures which ranged from true grain sizes (intercept length x 1.5) of 40 to 70 μm, and corresponding Vickers microhardness values ranging from about 110 VHN to 87 VHN (1.1 to 0.87 GPa); using either a 100 or 200 gf load. The grain structures in starting plates and cones, as well as in specimen segments extracted from deformed and recovered samples were examined by light metallography (LM) by cutting, mounting, grinding and polishing, and finally etching to reveal microstructural details in a solution of 1 part HNO_3, 2 parts HCl, and 4 parts HF at ice temperature (~0°C). Corresponding specimens were prepared for transmission electron microscopy (TEM) by extracting 3 mm discs which were ground, dimpled, and electropolished to electron transparency in a Struers Tenupol-3 jet polisher using a solution consisting of 10 parts methanol, 2 parts glycerin, 2 parts sulfuric acid, 1 part hydrofluoric acid, and 5 parts ethanol by volume; using a polishing voltage between 12 and 8 volts at a temperature of about 8°C. A Hitachi H-8000 analytical TEM was operated at 200 kV, and employed a double-tilt stage.

Tantalum
Edited by E. Chen, A. Crowson,
E. Lavernia, W. Ebihara, P. Kumar
The Minerals, Metals & Materials Society, 1996

Results and Discussion

Plane-Wave Shock Loading of Ta Plate

Since shock loading at different oblique angles relative to the liner plates constitutes the initial (precursor) event in the shaped charge or self-forging process, an examination of a plane-wave, shock-loaded Ta plate (8 mm thick) provides a starting point in this microstructure chronology. Figure 1 shows typical, comparative views of the starting Ta liner (plate) materials along with an example of a shock-loaded (at 45 GPa peak pressure; 1.8 μs pulse duration (7)) plate (~43 μm grain size; 110 VHN). Deformation twins evident in both Fig. 1(c) and (d) are a common microstructure feature, and provide for significant shock hardening (176 VHN in constrast to 110 VHN cited above). Murr, et al (8) have shown that twinning in Ta is dependent upon the attendant strain, strain rate, temperature, and grain size; with the twin fraction increasing with increasing grain size. Since shock pressures associated with shaped-charge and EFP processes usually approximate or exceed the peak pressure of 45 GPa involved in the experiment represented in Fig. 1(c) and (d), it might be expected that deformation twins would be introduced as a precursor microstructure into the shaped-charge and EFP liners.

Residual Shaped Charge and EFP Microstructures

Figure 2 shows for comparison the corresponding shaped charge and EFP process schematics along with representative examples of recovered components: shaped charge slug and jet fragment, and an EFP slug. The shaped charge slug is an SEM image composite while the shaped charge jet fragment, and EFP slug are light micrographs. Both the shaped charge and EFP slugs exhibit varying degrees of surface erosion.

Figure 3(a) shows a quarter of the shaped charge slug transverse section at the region of maximum diameter (Fig. 2). The cross-section is characterized by a wavy microstructure which propagates from the edge inward, evolving near the slug center into a more equiaxed grain or sub-grain microstructure. Figure 3(b) to (d) illustrate the wavy microstructure features which consist of varying degrees of elongated and narrow dislocation cells whose misorientations change from <1° at the slug edge to ~10° at the slug center. Figure 4(a) shows the corresponding slug center to consist of equiaxed, recrystallized grains surrounded by a zone of even smaller grains and sub-grains. The TEM view in Fig 4(b) shows the (dynamically) recrystallized grain structure near the slug center having a mixture of misorientation angles ranging from about 6° to ~12°. Many boundaries exhibit dense dislocation wall (DDW) structures and are part of an evolutionary process involving a systematic division of the elongated, recovery-related cell structures in Fig. 3(c) and (d). The dynamically recrystallized microstructure core region in the slug represents only about 4% of the slug volume, with the balance of the microstructure representing systematically evolving recovery and dislocation cell microstructures. The microhardness is maximum near the mid-point between the edge and center (~215 VHN) and drops to 125 VHN at the slug center, indicative of dynamic recrystallization-related softening.

The corresponding Ta jet fragment cross section and center region is shown in Fig. 5 to be similar to the slug, but the cross-section does not evolve into a recovery microstructure (Fig. 5(a)), and consists of varying and often concentric zones of dynamically recrystallized, equiaxed grains and sub-grains. The misorientations are similar to those observed in the slug center (6° to ~12°). Correspondingly, and in contrast to the residual slug microstructure, the shaped charge jet fragments consist almost entirely of dynamically recrystallized grains. The micro-hardness does not vary much from 121 VHN near the jet fragment center (Fig. 5(b) and (c). In contrast to Fig. 1(a) and (b), the shaped charge slug and jet fragment zones exhibiting dynamic recrystallization have true grain sizes in the range of roughly 0.5 to 1 μm, which represents a reduction in grain size that approaches a factor of 10^2, since starting liner grain sizes averaged 53 μm.

Preliminary (annealing) studies of recrystallization and grain growth in Ta liner plates have shown that these phenomena commence around 1200° C or roughly 0.4 T_M (T_M is the melting temperature). It might be recalled that roughly 80% of the outer liner cone wall forms the shaped charge slug while the inner 20% forms the elongating and particulating jet. The single, recovered jet fragment volume shown in Fig. 2 is only about 2% of the total slug volume, and the corresponding maximum cross-section area for the jet fragment is only 4% of the slug. In addition, the cumulative true strain in the jet fragment is probably 6 to 9 compared to 3 to 4 in the slug (9). Consequently, the adiabatic jet heating is considerably higher and phenomenologically different from the slug, and this accounts for the dynamic recrystallization fraction difference in the slug and jet fragment. Because of the prominence of dynamic recrystallization in the jet fragments, it probably plays a major role in the jet elongation as discussed previously (2, 10). No melt phenomena or melt-related microstructures were observed in either the shaped charge slug or jet fragments examined.

The concept of dynamic recrystallization in the detonating and deforming shaped charge has continued to be a contentious issue. Very recent discussions by Lichtenberger (11) allude to the fact that the assumption of dynamic recrystallization during liner implosion would be particularly favorable to superplastic behavior of the jet as originally proposed by Chokshi and Meyers (10), but complete dynamic recrystallization cannot be achieved because of time limitations on diffusional phenomena, etc. However, it must be recognized that classical diffusional phenomena and other classical deformation behavior cannot possibly be invoked for the elongating jet. Furthermore, well-defined, equiaxed, recrystallized grains are observed in the recovered jet fragments as shown prominently in Fig. 4. In this regard, Hines and Vecchio (12) have recently also

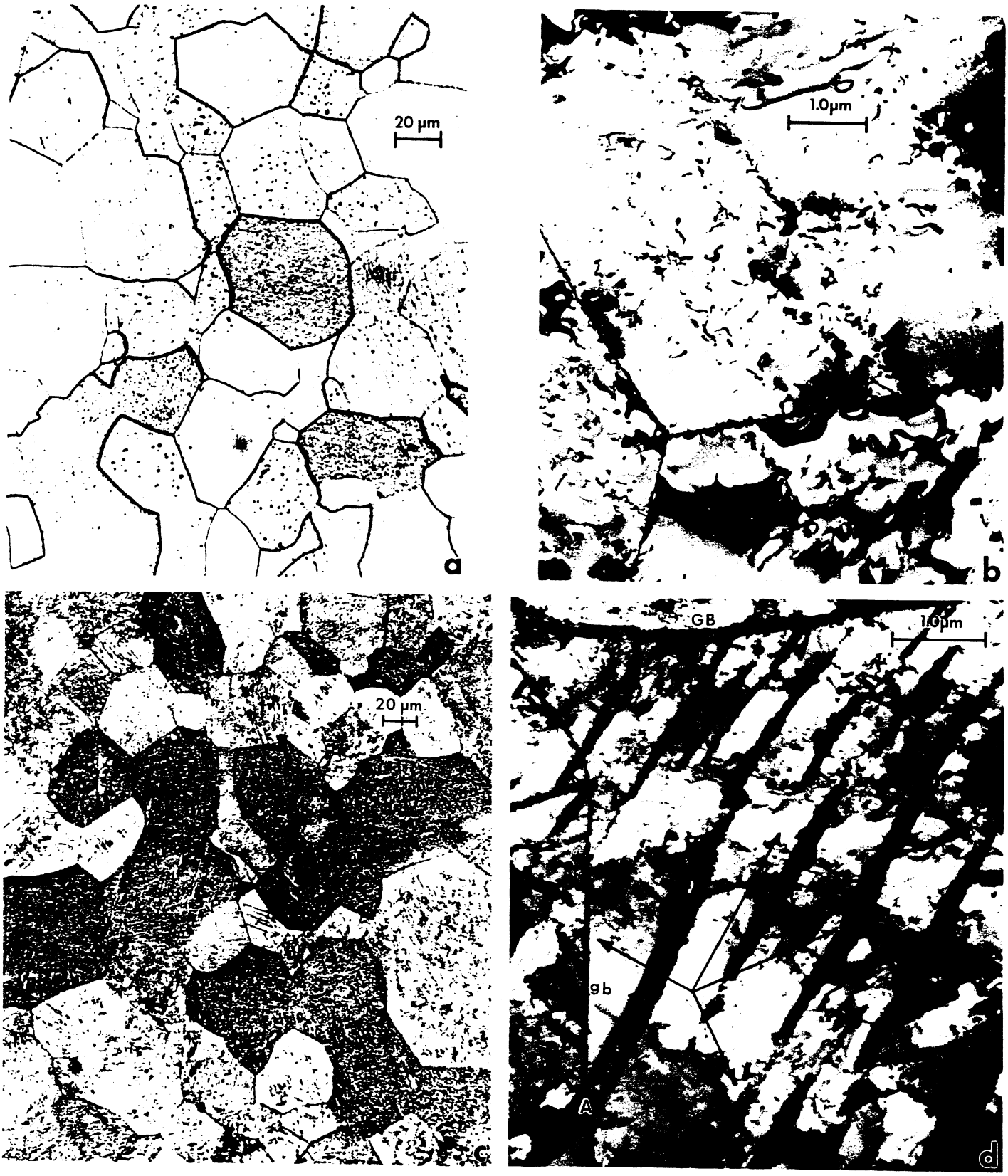

Fig. 1: Comparative views of starting Ta liner materials and plane-wave, shock-loaded Ta plate. (a) Light micrograph of typical Ta shaped charge (annealed) liner showing equiaxed grain structure. (b) Typical TEM view showing grain boundary triple point in liner material in (a). (c) Light micrograph of plane-wave, shock-loaded (45 GPa) Ta plate. (d) TEM image of deformation twins in (c). The grain surface orientation in (d) is (100). The principal <042> directions are shown by arrows. The twin boundaries lie along these trace directions coincident with {112} planes which make an angle of roughly 66° with the grain surface. Note high-angle grain boundary at GB and low-angle boundary at gb which is "sheared" as it crosses the deformation twin at "A".

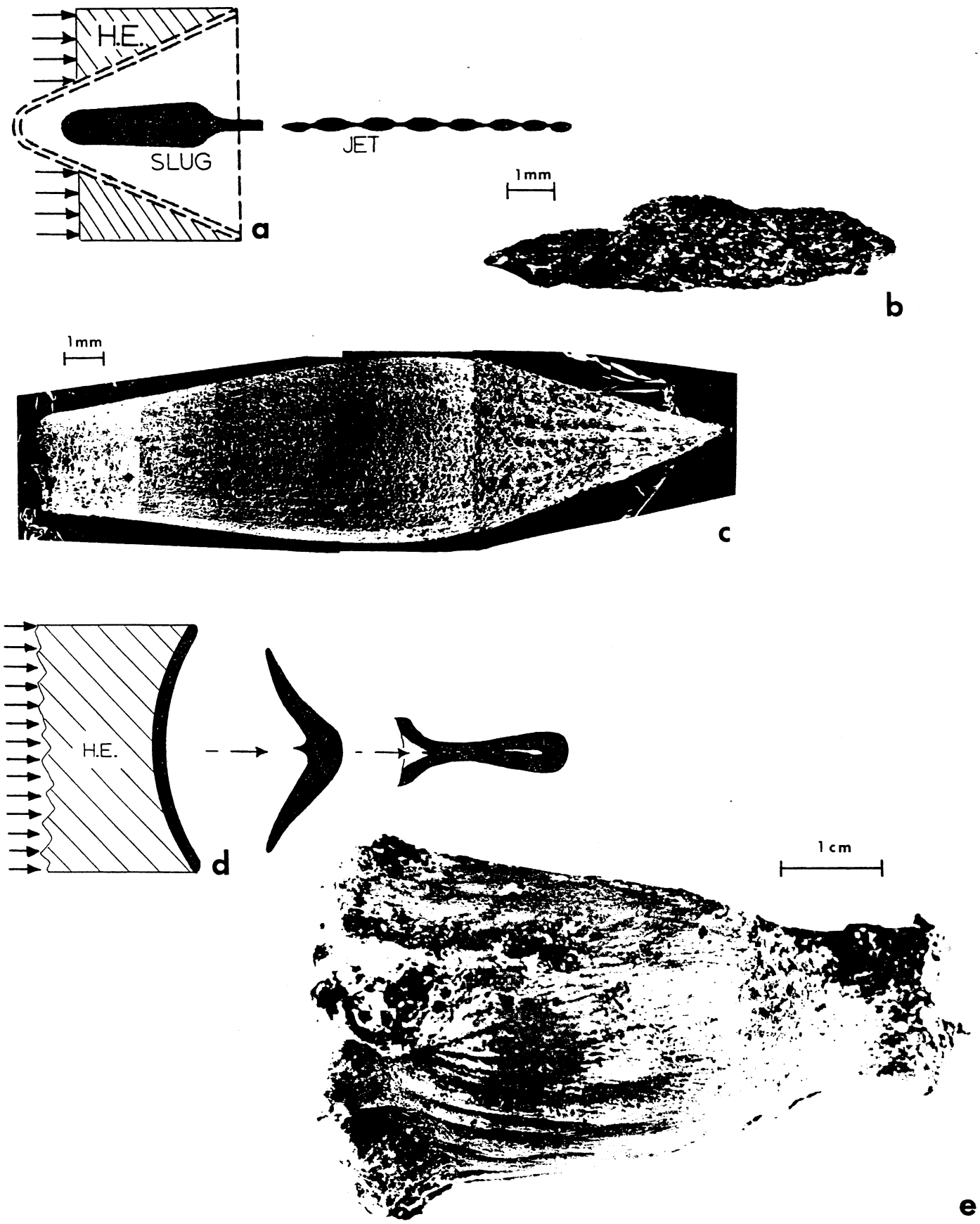

Figure 2: Tantalum shaped charge and EFP components. (a) Shaped charge schematic showing slug and jet formed from high-explosive (H.E.) detonated, collapsed cone (dotted). (b) Recovered jet fragment. (b) SEM composite view of recovered slug. (d) EFP formation schematic. (e) Recovered EFP. Note detonation (shock) front indicated by arrows in (a) and (d).

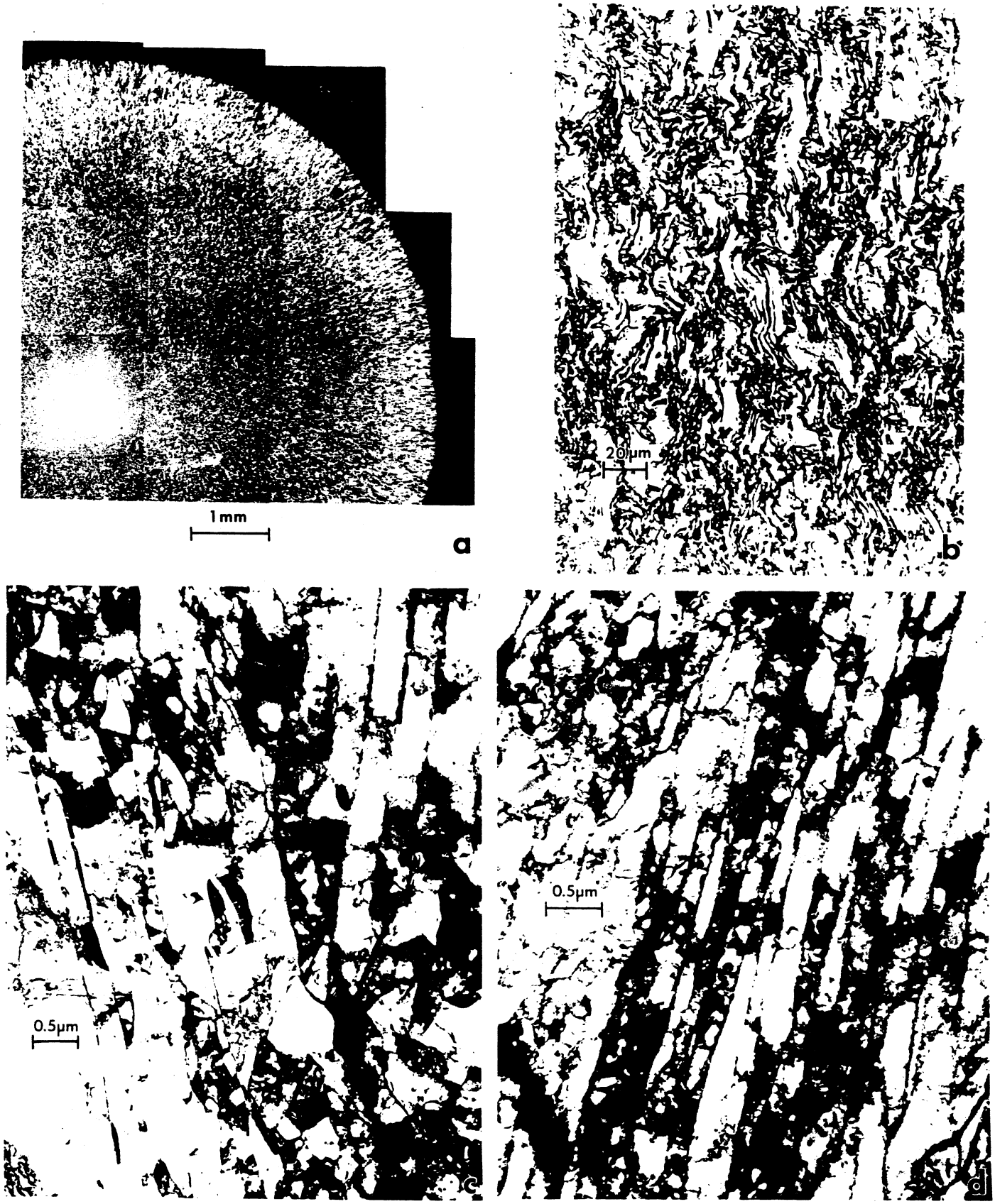

Figure 3: Cross-section views of recovered Ta shaped charge slug. (a) Light micrograph showing quarter section view of slug. (b) Light microscope view showing recovery structure approximately mid way between the center and edge in (a). (c) TEM view of elongated and other dislocation cell structures near the edge of the slug in (a). (d) TEM view of elongated dislocation cell structure corresponding to wavy features shown in (b) above.

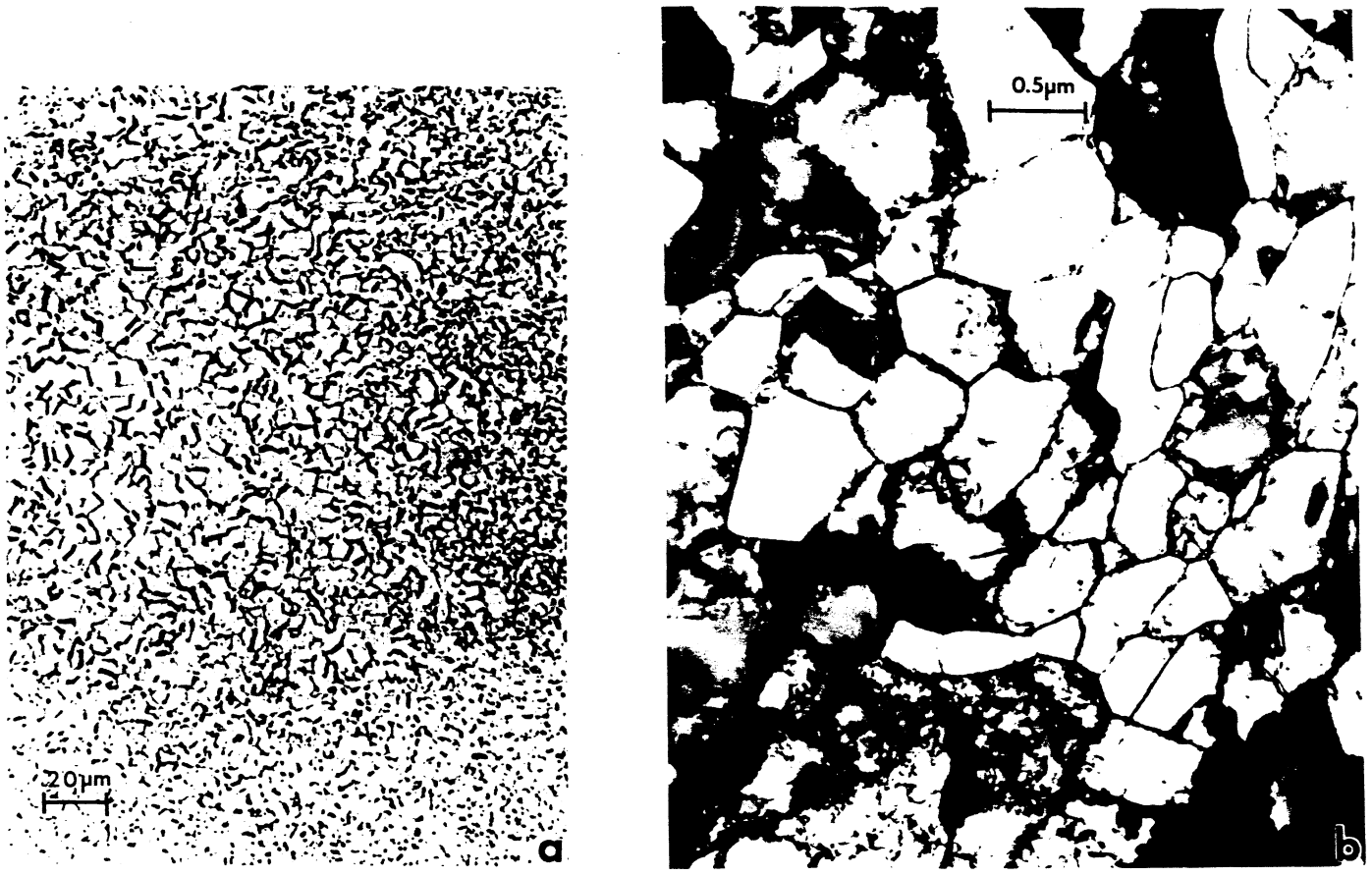

Figure 4: Slug cross-section center. (a) Magnified light microscope view of slug center in Fig. 3(a). (b) TEM view of slug center region in (a).

discussed the prospects for mechanically-assisted subgrain rotation as a mechanism of dynamic recrystallization in high strain and high-strain-rate regimes experienced in shaped charge jet elongation, shear-bands, and related regimes because diffusion, rate-controlled models applied specifically to recrystallization in shear bands could not justify any recrystallization behavior. Mechanically assisted recrystallization by sub-grain rotation, etc. is certainly not a new concept and has been especially attractive in explaining recrystallization phenomena at high strain rates (13, 14). If we accept the prospects for "mechanically" induced recrystallization, it might follow that so-called high-angle (of misorientation) recrystallized grain boundaries would necessarily follow the conditions observed for more conventional dynamic recrystallization. Consequently, this would explain the relatively smaller misorientation angles observed for recrystallized grains in the Ta shaped charge jet fragments in particular.

Figure 6 shows some representative microstructures corresponding to a diversity of regions within the recovered EFP shown in Fig. 2(e). The light microscope views shown in Fig. 6(a), (c), and (e) correspond to different regions on a longitudinal half-section of the recovered EFP, while the corresponding TEM images in Fig. 6(b), (d), and (f) represent thin sections sliced coincident to these representative surface sections. Figure 6(a) and (b) represent typical regions in the EFP tail and in portions near the head and mid-section while Fig. 6(c) and (d) represent regions in the inner tail regions. Note that this wavy (Fig. 6(c)) microstructure is similar to that found in the shaped charge slug in the mid-point zone between the center and edge (Fig. 3(b)). The corresponding TEM image in Fig. 6(d) is also similar to Fig. 3(d), but the cells are less elongated and are beginning to develop recrystallized segments (with misorientations between 4° and 6°). Figure 6(e) and (f) represent some of the most severe grain distortion/elongation. Figure 6(f) shows more recrystallized grains in contrast to Fig. 6(d), but the dynamically recrystallized regions in the EFP slug are not as obvious (with misorientations <9°) as those in the shaped charge jet and slug, and the volume fraction of recrystallized microstructures in the EFP are at least a factor 10 less than in the shaped charge slug. Consequently, dynamic recrystallization plays a negligible role in Ta EFP development in contrast to the Ta shaped charge slug or jet. The EFP is characterized by rather regular dislocation cell structures (Fig. 6(b)), elongated dislocation cells representing dynamic recovery microstructures, and scant evidence for dynamic recrystallization. We illustrate these features in a little more detail in Fig. 7 which shows an enlarged view of Fig.

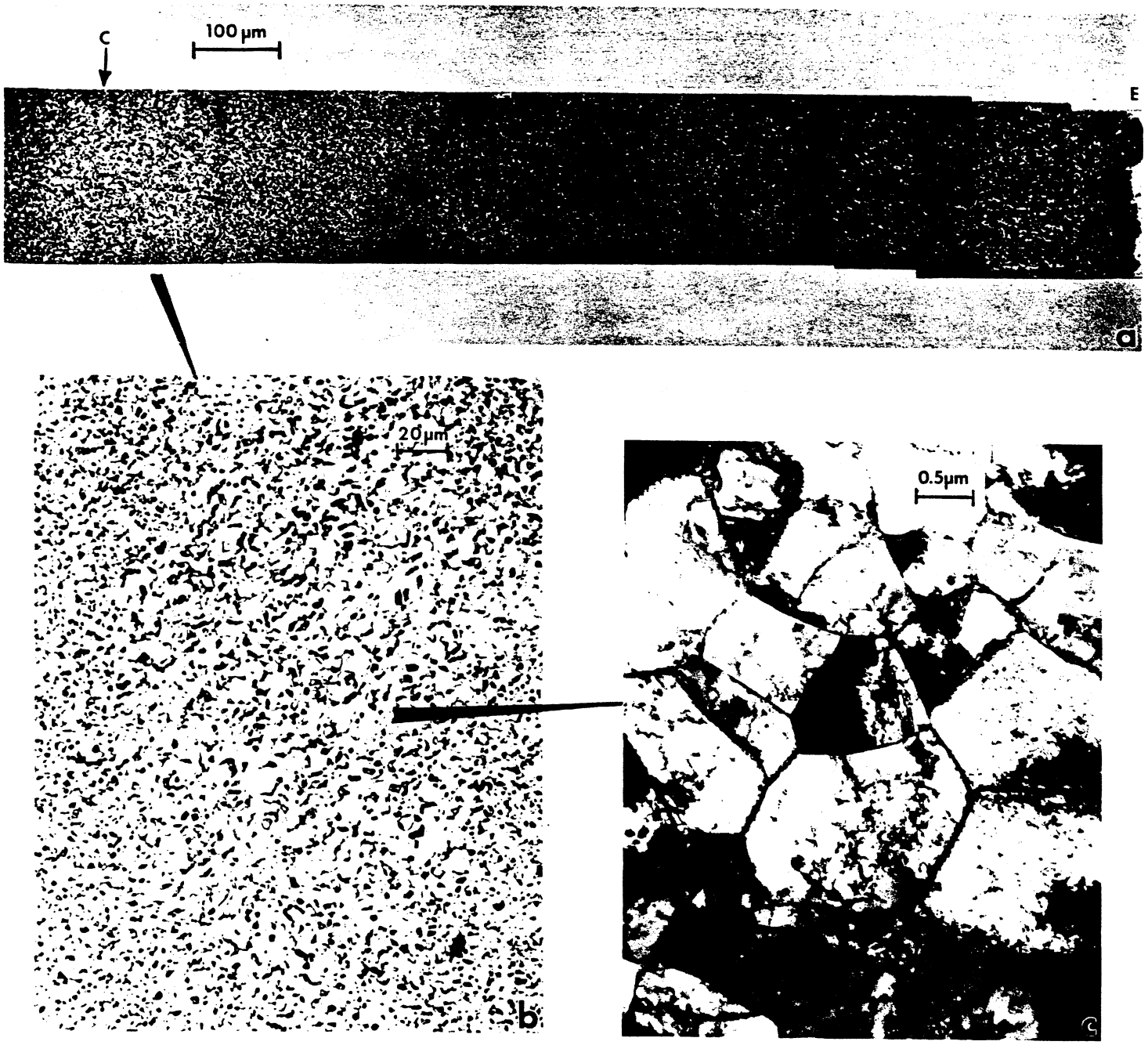

Figure 5: Jet fragment cross-section views. (a) Light micrograph composite showing a strip section from the jet center (C) to the outside edge (E). (b) Magnified light microscope view of jet fragment center in (a). (c) TEM bright-field electron micrograph typical of jet center region in (b).

6(d) with a selected-area electron diffraction pattern corresponding to a large area of the image, and showing a consistent misorientation of only 2° (Fig. 7(b)). These features are shown in contrast to a more equiaxed example of a recrystallized region where the grain orientations were either different from grain-to-grain, or exhibited misorientations which ranged between 4° and 9°; creating the prominent contrast differences observed in the bright-field image in Fig. 7(c).

Microhardness values in the EFP ranged from 144 VHN to 204 VHN. Consequently there is significant hardening everywhere in the EFP, in contrast to the starting liner (~87 to 95 VHN). In this context, there are no apparent "soft" regions within the EFP which can be unambiguously associated with recrystallization as in the shaped charge jet fragments and slug center. Consequently this is consistent with the intermixing of dynamic recovery and recrystallized microstructures and the dearth of recrystallized grains in the EFP.

It should also be noted that there were no deformation twin observations in either the recovered shaped charge components or the EFP. This is not unexpected in the

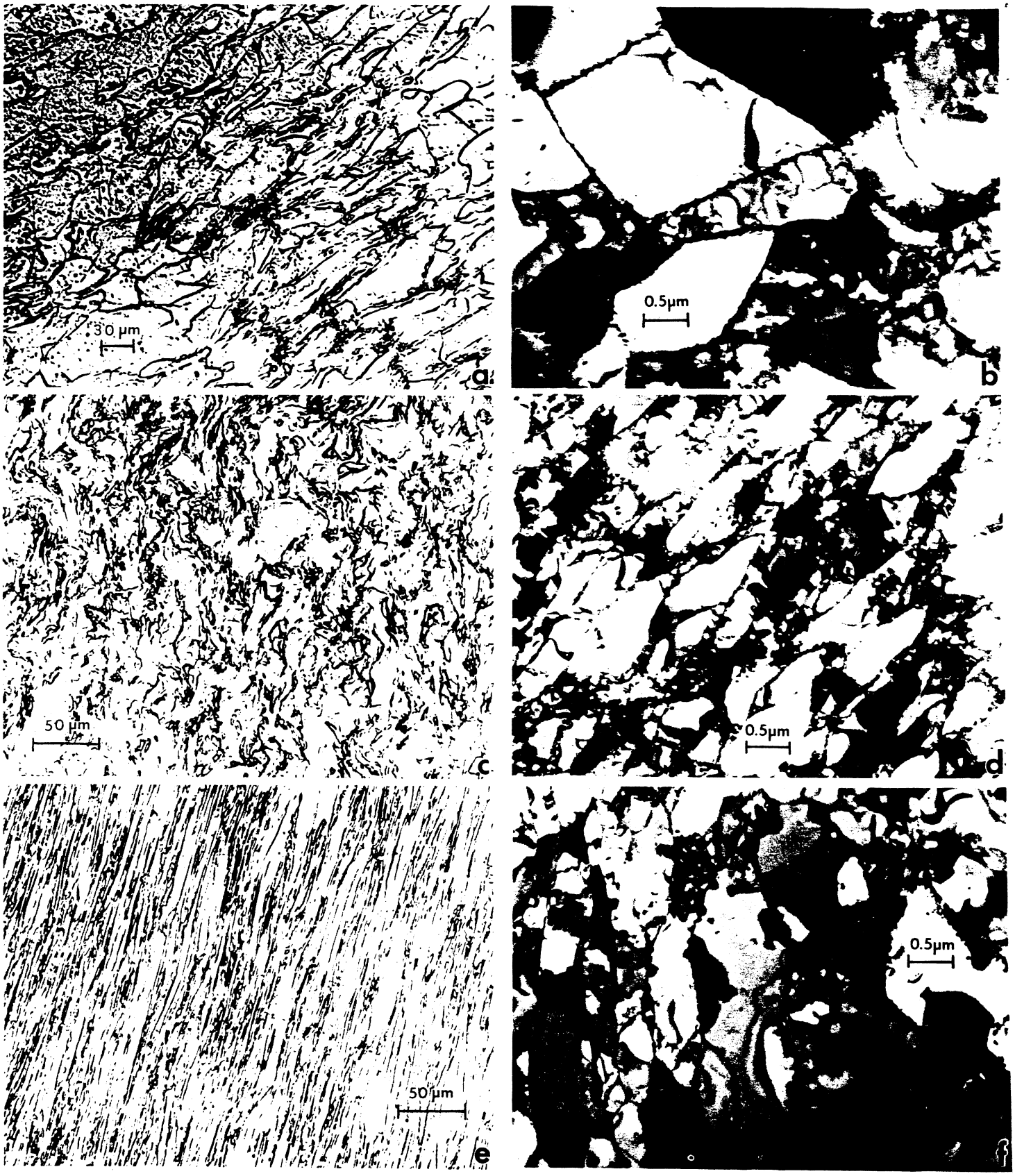

Figure 6: Examples of microstructure variations observed within the Ta EFP slug cross section. (a) Light microscope view showing lightly strained region typical of the tail regions. (b) TEM bright-field image corresponding to (a). (c) Light micrograph of moderate strain region showing wavy microstructure similar to shaped charge slug center (Fig. 3(b)). These zones occur throughout the EFP. (d) TEM bright-field image typical of (c). (e) Light micrograph showing severe deformation as evidenced by grain elongation/distortion near EFP center. (f) TEM image corresponding to (e).

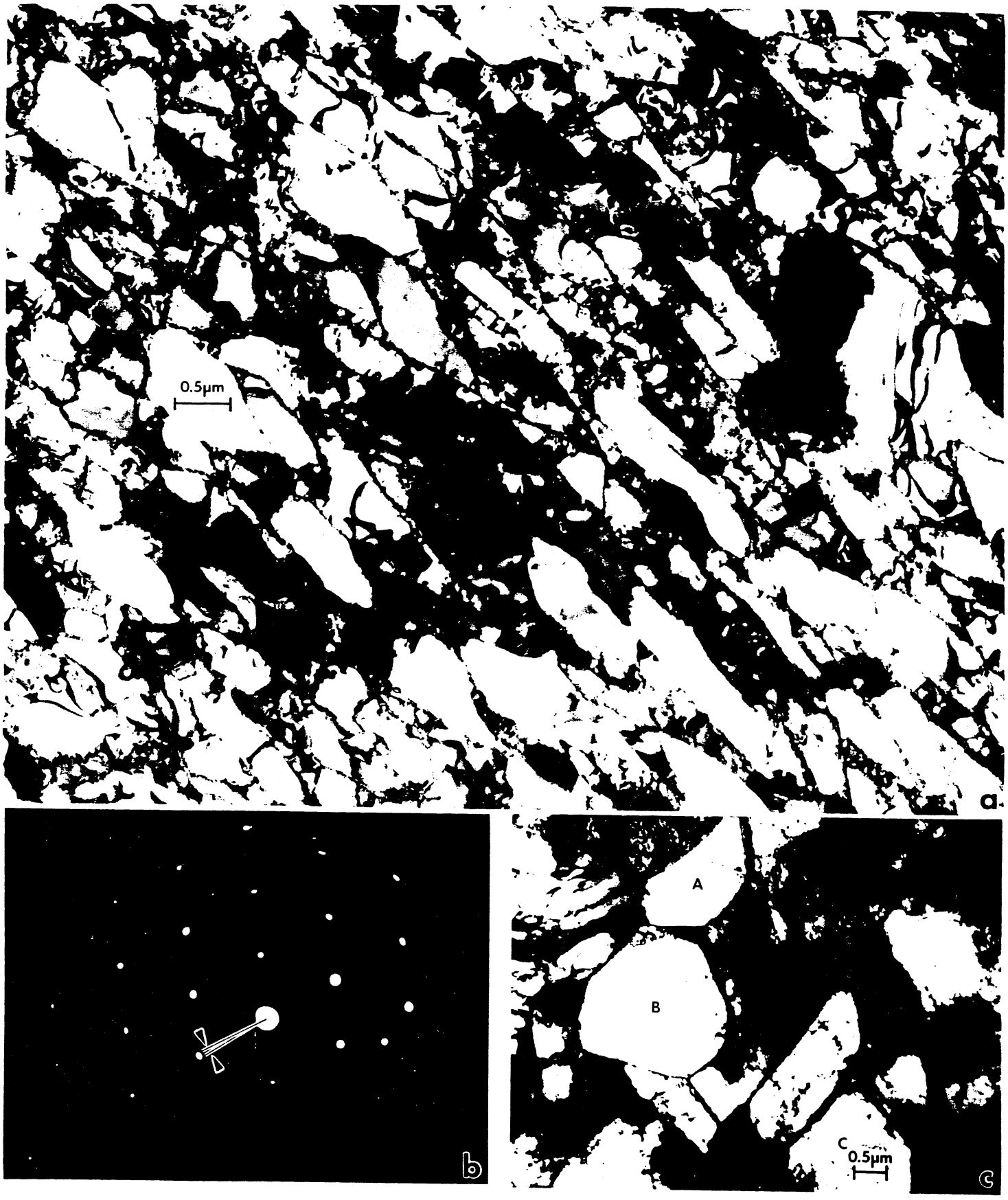

Figure 7: Comparison of elongated dislocation cell/recovery microstructures which dominate the EFP ((a) and (b)) along with isolated recrystallized regions (c). The SAD pattern in (b) shows the concept of measuring average microstructure misorientation angles and the nominal, 2° misorientation typical for microstructures in (a). Grains marked A, B, C have different grain surface orientations.

shaped charge since the extreme strains and adiabatic heating either annihilate any twins which would be formed by the initial shock loading of the liner, or they contribute directly to recovery and recrystallization and are annihilated. However, since the EFP is not so severely deformed, twins were expected in those regions where the self-forming strains were low, and the associated adiabatic heating would be expected to be small. The lack of any twins in the EFP may result by lower than expected shock pressures or a high thermal sensitivity of deformation twins in Ta which would rapidly and completely annihilate them if the EFP became sufficiently hot during self-forging. Because of their irregular boundaries and associated defect structures (dislocations in the twin interface, etc.) deformation twins as shown in Fig. 1(d) may be high energy microstructures and highly thermal sensitive. This was noticed in recent experiments involving dynamic (Hopkinson Bar) compression (at 10^3 s^{-1} to a dynamic strain of -0.26) of the shock-loaded sample in Fig. 1(d). After straining the twins became very short segments in many grains and typical of recovery phenomena (8). It was also noted that the test elevated the specimen temperature several hundred degrees. Finally, as this paper was completed, we observed some peculiar deformation twins in sections of a Ta-2.5% W EFP which, in contrast to deformation twins in the starting Ta-2.5% W liner similar to those shown for Ta in Fig. 1(d), appeared to have "recovered". That is, the twins became small elliptical "grains" with essentially no dislocations inside, and with well-defined, but irregular interfaces. SAD patterns contained very prominent twin reflections as well. These features, as we noted earlier, seem to point to a severe thermal instability of deformation twins in Ta and dilute alloys such as Ta-2.5% W.

Summary

While deformation twins have been observed in plane-wave, shock-loaded tantalum (~43 μm grain size), they are not observed in either residual shaped charge jet and slug microstructures or in recovered EFP's. Shaped charge jet fragments are characterized by either a uniform, small grain structure or concentric zones of varying grain sizes which are, in the extreme, roughly a factor 10^2 smaller than the starting liner grain sizes. These features attest to the dominant role that dynamic recrystallization plays in shaped charge jet development. Correspondingly, shaped charge slug microstructures exhibit a central core of dynamically recrystallized material with a radiating zone of dynamic recovery microstructures with boundary misorientations which increase from <1° at the slug perimeter to >6° near the central core. By contrast, the EFP is characterized by microstructures dominated by dislocation cells and elongated dynamic recovery features (dislocation cells) with increasing strain, and a low incidence of dynamically recrystallized, small grains and sub-grains. Consequently, tantalum EFP's are characterized by strain-related dislocation (cell) structures which evolve and vary with strain localization.

Figure 8 illustrates a simple schematic comparison summarizing the observations of (dynamic)

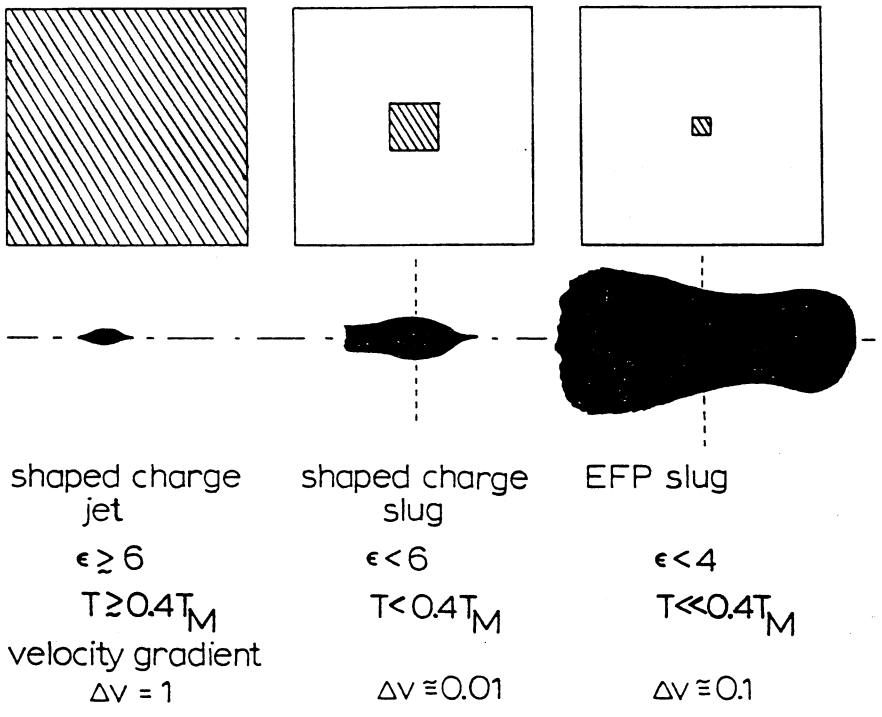

Figure 8: Schematic summary of shaped charge and EFP component regimes and approximate recrystallization fraction (shown shaded) in a typical, equivalent cross section.

recrystallization and the probable prominence or role it plays in deformation-related development of these corresponding regimes. These regimes are phenomenologically the same as those described for thick-wall Ta cylinder tests by Meyers, et al (15): dislocation/cells at low strains; dynamic recovery structures at moderate strains; dynamic recrystallization at high strains (true strains >6). It is apparent that EFP development can be adequately modeled by rather conventional dislocation phenomena, including strain-related dislocation density changes and microstructure evolution. In contrast, the shaped charge jet development requires a very different model. In the case of Ta, twinning does not appear to play a significant role in either the shaped charge or the EFP development and performance and as a consequence does not appear to be a necessary model consideration.

Acknowledgments

This research was supported in part by Department of the Army contract DAAA-21-94-C-0059 through the U.S. Army Research, Development and Engineering Center, Picatinny Arsenal, N.J., and a Mr. and Mrs. MacIntosh Murchison Endowed Chair (L.E.M.). We are also grateful to Dr. Lou Zernow who provided the recovered shaped charge components examined in this investigation, and Mike Hespos who provided the EFP components.

References

1. L. E. Murr, H. K. Shih, C-S. Niou, and L. Zernow, Scripta Metall. et Materialia, 29 (1993) 567.

2. L. E. Murr, H. K. Shih, and C-S. Niou, Materials Characterization, 33 (1994) 65.

3. L. E. Murr, C-S. Niou, and C. Feng, Scripta Metall. et Materialia, 31 (3) (1994) 297.

4. L. E. Murr, C-S. Niou, J. C. Sanchez, H. K. Shih, L. DuPlessis, S. Pappu, and L. Zernow, J. Mater. Sci., 30 (1995) 2747.

5. S. Pappu, C-S. Niou, C. Kennedy, and L. E. Murr, "A Study and Comparison of Microstructures in Ta and Ta-W Starting Liners and a Pure Ta Explosively Formed Penetrator", Microstructural Science, Vol. 23, ASM International, Materials Park, OH, in press (1996).

6. S. Pappu, C-S. Niou, C. Kennedy, L. E. Murr, L. DuPlessis, and M. A. Meyers, Chap. 59 in Metallurgical and Materials Applications of Shock-Wave and High-Strain-Rate Phenomena, L. E. Murr, K. P. Staudhammer, and M. A. Meyers (Eds.), Elsevier Science, B.V., The Netherlands, 1995, p. 495.

7. M. A. Meyers, Dynamic Behavior of Materials, Wiley Interscience, New York, 1994.

8. L. E. Murr, M. A. Meyers, C-S. Niou, Y. J. Chen, S. Pappu, and C. Kennedy, Acta Metall. et Materialia, in press (1996).

9. F. I. Grace, Chap. 45 in Shock-Wave and High-Strain-Rate Phenomena in Materials, M. A. Meyers, L. E. Murr, and K. P. Staudhammer (Eds.), Marcel Dekker, Inc., New York, 1992, p. 493.

10. A. H. Chokshi and M. A. Meyers, Scripta Metall. et Materialia, 24 (1990) 605.

11. A. Lichtenberger, Chap. 55 in Metallurgical and Materials Applications of Shock-Wave and High-Strain-Rate Phenomena, L. E. Murr, K. P. Staudhammer, and M. A. Meyers (Eds.) Elsevier Science, B.V. Amsterdam, 1995, p. 463.

12. J. A. Hines and K. S. Vecchio, Chap. 50, *ibid,* p. 421.

13. J. Flaquer and J. Gil Sevillano, J. Mater. Sci., 19 (1984) 423.

14. J. Gil Sevillano, P. van Houtte, and E. Aernoudt, Prog. Mater. Sci., 25 (1981) 69.

15. M. A. Meyers, V. F. Nesterenko, Y. J. Chen, J. C. LaSalvia, and M. P. Bondar, Chap. 58 in Metallurgical and Materials Applications of Shock-Wave and High-Strain-Rate Phenomena, L. E. Murr, K. P. Staudhammer, and M. A. Meyers (Eds.), Elsevier Science, B.V., Amsterdam, 1995, p. 487.